Acta Crystallographica Section D
Biological Crystallography
ISSN 0907-4449

A low-resolution structure of rice dwarf virus determined by *ab initio* phasing

Hisashi Naitow,[a] Yukio Morimoto,[b] Hiroshi Mizuno,[c] Hiromi Kano,[c] Toshihiro Omura,[d] Mika Koizumi[c] and Tomitake Tsukihara[a]*

[a]The Institute for Protein Research, Osaka University, 3-2 Yamada-oka, Suita 565, Japan, [b]The Department of Life Science, Faculty of Science, Himeji Institute of Technology, Kamigohri Akoh, Hyogo 678-12, Japan, [c]National Institute of Agrobiological Resources, Tsukuba Science City, Ibaraki 305, Japan, and [d]National Agriculture Research Center, Tsukuba Science City, Ibaraki 305, Japan

Correspondence e-mail: tsuki@protein.osaka-u.ac.jp

Received 7 November 1997
Accepted 29 May 1998

Rice dwarf virus crystals belong to space group *I*222 with cell parameters $a = 770$ (2), $b = 795$ (5), $c = 814$ (5) Å and $\alpha = \beta = \gamma = 90^\circ$. The unit cell of the crystal contains two viruses at the origin and body-centred positions. Using data synthesized from a rice dwarf virus model crystal in the space group *I*222, the possibility of *ab initio* phasing was thoroughly examined. The centric nature of the initial phases was unexpectedly broken by extensive iteration of the non-crystallographic symmetry averaging. The structure of rice dwarf virus was then solved with *ab initio* phasing up to 20 Å resolution. The triangulation number determined by the present study is $T = 13$, which is different from the triangulation number, $T = 9$, previously determined by electron microscopy [Uyeda & Shikata (1982). *Ann. Phytopathol. Soc. Jpn*, **48**, 295–300].

1. Introduction

Crystal structure analyses of biological macromolecules are usually initiated using the multiple isomorphous-replacement (MIR) method (Green *et al.*, 1954) or the molecular-replacement (MR) method (Rossmann, 1972). Initial phases of virus crystals determined by the MIR method, such as tomato bushy stunt virus (TBSV; Harrison *et al.*, 1978) and southern bean mosaic virus (SBMV; Abad-Zapatero *et al.*, 1981), or by the MR method, such as polyoma virus (Rayment *et al.*, 1982, 1983), mengovirus (Luo *et al.*, 1987), foot-and-mouth disease virus (Acharya *et al.*, 1989) and coxsackievirus B3 (Muckelbauer *et al.*, 1995), were refined using non-crystallographic symmetry averaging (NCSA), which has a large radius of convergence (Rossmann, 1990). In the case of bacteriophage MS2 (Valegård *et al.*, 1990), the initial phases determined at 8 Å resolution by the MR method with a completely unrelated model were successfully refined and extended to 3 Å resolution by using icosahedral NCSA.

Rossmann has suggested that *ab initio* phasing initiated by a hollow-shell model may be a useful method for the crystal structure analysis of spherical viruses (Rossmann, 1990). He and his coworkers have successfully applied this method to the structure determination of canine parvovirus (Chapman *et al.*, 1992; Tsao, Chapman & Rossmann, 1992). In this method, the size and position of the spherical shell are initially determined, and the initial phases calculated from the crystal structure of the spherical shell at low resolution are then refined and extended to higher resolution by the NCSA. A spherical shell has a centre of symmetry. When there are one or two spherical shells in the unit cell, the initial phases inevitably exhibit a centric distribution, because the unit cell always has a centre of symmetry at the centre of the shell or at the midpoint of the

two shells. Breaking the centre of symmetry of the initial phases is a serious problem for the crystal structure analysis.

In the case of canine parvovirus, space group $P2_1$, two spherical shells with outer and inner radii of 149 and 105 Å, respectively, at positions (0.25, 0.25, 0.25) and (0.75, 0.75, 0.75) in the unit cell, cause the initial phases to have a centre of symmetry (Tsao, Chapman & Rossmann, 1992). The centre of symmetry was successfully broken using NCSA, as one of the crystallographic symmetry axes is inclined by 2.5° to an icosahedral symmetry axis of the virus (Tsao, Chapman, Wu *et al.*, 1992; Tsao, Chapman & Rossmann, 1992). The crystal of SBMV belongs to space group *R*32 and has a virus particle at the origin. Each of the crystallographic axes at the origin is coincident with an icosahedral symmetry axis of the SBMV particle. The centric nature of the initial phase calculated with the spherical-shell model could not successfully be broken by NCSA (Johnson *et al.*, 1976). Thus, breaking the centre of symmetry was considered to be impossible when all crystallographic symmetry axes are coincident with symmetry axes of the virus.

Rice dwarf virus (RDV) belongs to the family *Reoviridae*, the genus Phytoreovirus, and infects rice, wheat, barley and insects of the *Nephotettix* species. The RDV exhibits a multi-shelled structure (Kimura & Shikata, 1968) consisting of a capsid outer shell and a core inner shell. The molecular weight of RDV is estimated to be 6.52×10^7 Da by small-angle neutron scattering, and the RNA content is approximately 20% of the total weight (Inoue & Timmins, 1985). The capsid outer shell and the core inner shell are estimated to be about 360 Å in radius with 85 Å thickness and 275 Å in radius with 35 Å thickness, respectively, by small-angle neutron scattering methods (Inoue & Timmins, 1985) and electron microscopy (Omura & Inoue, 1985). The RDV has 12 genome segments of dsRNA in the core inner shell (Omura & Inoue, 1985) and was reported to have six structural proteins (P1, P2, P3, P5, P7 and P8) detected in the purified virus preparations. P1 is considered to be an RNA-dependent RNA polymerase (Suzuki *et al.*, 1992). P2, which is essential for the RDV infection of insect cells (Yan *et al.*, 1996), is removed from the RDV particles by CCl_4 treatment during the virus purification process (Omura *et al.*, 1982). The RDV used in this study therefore lacks P2. P3 is the major protein in the core inner shell (Kano *et al.*, 1990). P5 is guanylyltransferase, which is involved in the mRNA capping reaction (Suzuki *et al.*, 1996). P7 is an RNA binding protein (Omura *et al.*, unpublished results). P8 (46 kDa; Omura *et al.*, 1989) is located on the surface of the capsid outer shell. The number of morphological units on the capsid outer shell was estimated to be 180 from electron microscopy (Kimura & Shikata, 1968; Uyeda & Shikata, 1982). If a morphological unit consists of a trimer of P8, then 540 identical protein molecules are assumed to be arranged on the capsid outer shell with $T = 9$ icosahedral quasi-symmetry (Caspar & Klug, 1962).

In spite of extensive studies of RDV by various methods, more precise structural studies are needed to confirm morphological features such as the triangulation number. As described later, the RDV crystal has one particle at the origin and one particle at the body-centred position in its unit cell. The initial phases calculated from the spherical-shell model are centric and each of the crystallographic axes coincides with an icosahedral symmetry axis of RDV, as in the case of SBMV. Therefore, the *ab initio* phasing of the RDV crystal was expected to be impossible according to Johnson *et al.* (1976). However, we reinspected the possibility of breaking the centric nature of model crystals by icosahedral NCSA and applied NCSA to the structure determination of RDV at 20 Å resolution.

2. Structure determination of model crystals

2.1. Construction of model crystals

We selected bovine leucine aminopeptidase, molecule 1LAP (Jurnak *et al.*, 1977), from the Protein Data Bank (Bernstein *et al.*, 1977) as a construction unit for the model crystals. The molecular weight of 1LAP is similar to that of P8, a coat protein of the capsid outer shell of RDV (Omura *et al.*, 1989). The length of the major axis of the 1LAP molecule resembles the thickness of the capsid outer shell of RDV, 85 Å (Omura & Inoue, 1985). 1LAP molecules were spherically arranged in order to construct model viruses with either $T = 9$ or $T = 13d$ icosahedral quasi-symmetries. The crystallographic parameters were set with the space group *I*222 and the cell dimensions $a = 789$, $b = 789$ and $c = 789$ Å. Totals of 606018 and 945468 independent atoms were generated in the crystallographic asymmetric unit for $T = 9$ and $T = 13d$ model crystals, respectively. The structure factors of the model crystals with $T = 9$ and $T = 13d$ model viruses were calculated up to 30 Å resolution with their atomic parameters each having a temperature factor of $B = 100$ Å^2. The structure-factor amplitudes of each model crystal were artificially included with average 10% random errors.

2.2. *Ab initio* phasing with model crystals

Tsao *et al.* (1992) have demonstrated the feasibility of using NCSA and an initial spherical-shell model using simulated data calculated from arbitrary models. Following their proposed *ab initio* phasing, similar studies were extended to test the feasibility under more stringent conditions, where each crystallographic twofold axis was coincident with the icosahedral symmetry, and to demonstrate that it was possible to distinguish $T = 9$ and $T = 13d$ model viruses using only a spherical-shell model and the $T = 1$ icosahedral symmetry. Success encouraged us to proceed with the *ab initio* phasing of RDV by similar starting models.

3. Structure determination of RDV

3.1. X-ray experiments

The crystallization method and morphology of the RDV crystals were described by Mizuno *et al.* (1991). Once the crystals are removed from the mother liquor, they deteriorate rapidly. Therefore, the crystals were mounted in a tapered capillary filled with mother liquor. All X-ray experiments with the RDV crystals were undertaken at the Photon Factory (PF)

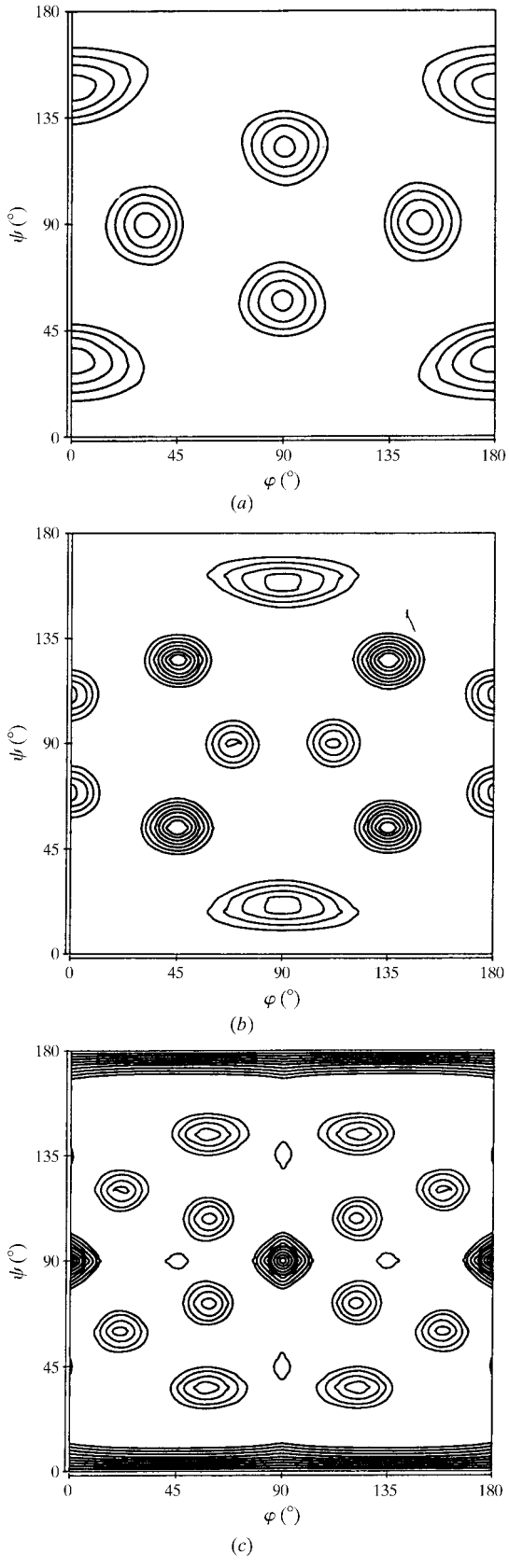

Figure 1
The rotation-function sections of (*a*) $\kappa = 72^\circ$, (*b*) $\kappa = 120^\circ$ and (*c*) $\kappa = 180^\circ$ in a polar coordinate system. The calculation was carried out by the slow rotation-function algorithm with the program *X-PLOR*.

of the National Laboratory for High Energy Physics (KEK) in Tsukuba, Japan, using a Weissenberg camera designed especially for macromolecules (Sakabe, 1983) and equipped with a Fuji imaging plate (Miyahara *et al.*, 1986).

We processed ten data sets of RDV with the program *DENZO* (Otwinowski, 1993). Cell constants are a = 770 (2), b = 795 (5), c = 814 (5) Å and $\alpha = \beta = \gamma = 90^\circ$. RDV crystal diffraction intensity statistics restrict the space group to either $I222$ or $I2_12_12_1$. Only full reflections of the 239 frames from the ten crystals were scaled and merged together to obtain the observed structure-factor amplitudes of RDV. A total of 786381 reflections with $I > \sigma(I)$ from the ten data sets were combined to produce the 10 Å native data set with a completeness of 95.1% and an $R_{\rm merge}$ [$R_{\rm merge} = \sum |\langle I(hkl)\rangle - I_i(hkl)| / \sum \langle I(hkl)\rangle$] of 18.7% for 128221 independent reflections (averaged redundancy of 6.0). 4001 reflections, corresponding to 0.5% of the total reflections observed, were rejected from scaling and averaging to generate the observed independent reflections.

3.2. Orientation of the virus particles in the unit cell

The unit-cell volume and the molecular weight of RDV give V_m values of 3.8 and 1.9 Å^3 Da^{-1} for two and four virus particles in the unit cell, respectively. Both values are slightly outside the range of 2.2–3.5 Å^3 Da^{-1} observed for other virus crystals. Assuming the space group $I222$, we may locate two spherical particles with radii of 343 Å in the unit cell without any overlap of virus particles. The two particles occupy 68% of the unit cell by volume. On the other hand, the unit cell of $I2_12_12_1$ should contain at least four particles. Since the volume of the particles is approximately 1.36 times the volume of the unit cell, they cannot pack well in the unit cell. Consequently, the space group of RDV was restricted to $I222$.

Orientation of RDV in the crystal is restricted to the two cases in which three twofold axes of RDV coincide with the crystallographic twofold axes. The self-rotation function (Rossmann & Blow, 1962) was calculated with an integration radius of 400 Å using all the observed reflections lower than 20 Å resolution. Three sections of κ = 72, 120 and 180° are given in Figs. 1(*a*), 1(*b*) and 1(*c*). The peaks of these sections clearly show icosahedral symmetries and confirm that RDV is an icosahedral virus. The constellation of the symmetry elements established the particle orientation.

3.3. Starting model for RDV

The outer and inner radii of a spherical-shell model were determined by a two-dimensional *R*-factor search. The diffraction data from 100 to 50 Å resolution were used for the *R*-factor search, because observed structure-factor amplitudes lower than 100 Å resolution were not reliable and those of resolution higher than 50 Å do not have the spherical-shell property (Fig. 2).

RDV contains double-stranded RNA in the core inner shell. The RNA in a virus is usually disordered so that its contribution to the structure factors is negligible at high resolution. However, in the present case, the resolution is so low that the

contribution of the RNA to the structure factors may not be negligible. A relative electron density can be defined as $\rho'_{NA} = (\rho_{NA}/\rho_P)$, where ρ_{NA} is the density of the RNA and ρ_P is that of the protein (Chapman *et al.*, 1992). Since the electron density of the protein is lower than that of the RNA, the relative electron density is larger than one (Chapman *et al.*, 1992). Setting the relative electron density to a constant value from 1.1 to 1.6 in 0.1 steps, we independently carried out two-dimensional *R*-factor searches with the inner and outer radii. The best *R* factors were obtained at the relative electron density $\rho'_{NA} = 1.4$ (Fig. 3). The outer and inner radii corresponding to local minima 1 and 2 shown in Fig. 3 are reasonable candidates for the starting models ($\rho'_{NA} = 1.4$) for RDV, because they are approximately consistent with the radial distribution of observed structure amplitudes lower than 50 Å given in Fig. 2, the radii obtained from electron microscopy (Omura *et al.*, 1989) and neutron scattering (Inoue & Timmins, 1985), within ±10% errors.

In order to establish the starting resolution for the *ab initio* phasing, we compared the radial distribution of the structure-factor amplitudes of the observed reflections and the Fourier transforms of two candidates. The radial distribution of the model for the local minimum 2 agrees well with that of the observed reflections at resolutions lower than 50 Å, as shown in Fig. 2. Thus, the starting resolution of phase refinement by NCSA was set to 50 Å resolution.

3.4. *Ab initio* phasing

Electron density calculated from the observed structure-factor amplitudes phased by each starting model of local minima was averaged over the 15 non-crystallographic symmetry operations of the icosahedron in the crystallographic asymmetric unit of the space group *I*222. Solvent flattening was applied to the solvent region and the RNA region independently, and the electron-density values of the solvent and the RNA regions were replaced by their respective averaged values. The averaged electron-density map was used to generate phase angles at 50 Å resolution. A new electron-density map was calculated at the same resolution with the calculated phase angles and the observed structure-factor amplitudes modified by the simple weighting scheme (Rayment *et al.*, 1982). After 150 iterations of this NCSA procedure, the *R* factor and the correlation coefficient between the observed and the calculated structure-factor amplitudes converged to 0.271 and 0.896, respectively, for the starting model of the local minimum 1, and were 0.277 and 0.884, respectively, for that of the local minimum 2. The averaged difference between the two resultant phase sets was as small as 20° at 20 Å resolution and the two electron-density maps were difficult to distinguish from each other. The NCSA calculations for the local minima 3, 4, 5, 6, 7 and 8 resulted in *R* values significantly higher than that for the local minimum 2. Their electron-density maps were poor in virus-shell shape in comparison with those for the local minimum 2. Consequently, the model for the local minimum 2 was used for an initial structure of phase extension.

An electron density calculated at 50 Å resolution (Fig. 4*a*) clearly shows $T = 13$ icosahedral quasi-symmetry on the capsid outer shell of RDV. The electron density of the capsid outer shell is high at the quasi-threefold axes and is low at the icosahedral fivefold and quasi-sixfold axes. This icosahedral quasi-symmetry of $T = 13$ completely conflicts with the evidence from electron microscopy of RDV, which indicated

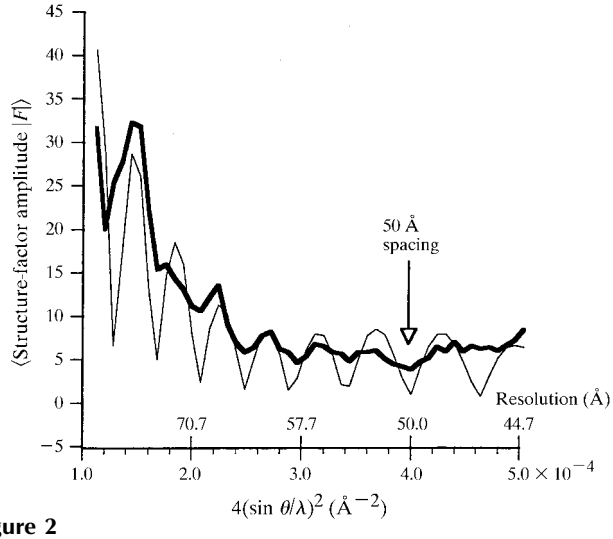

Figure 2
The radial distibution of the observed structure-factor amplitudes of the RDV crystal and that of the spherical-shell model for the local minimum 2 in Fig. 3 are shown by a heavy and a thin line, respectively. The averaged structure-factor amplitude in each resolution shell is plotted in arbitrary units as a function of $4(\sin\theta/\lambda)^2$ and resolution. An arrow shows 50 Å spacing.

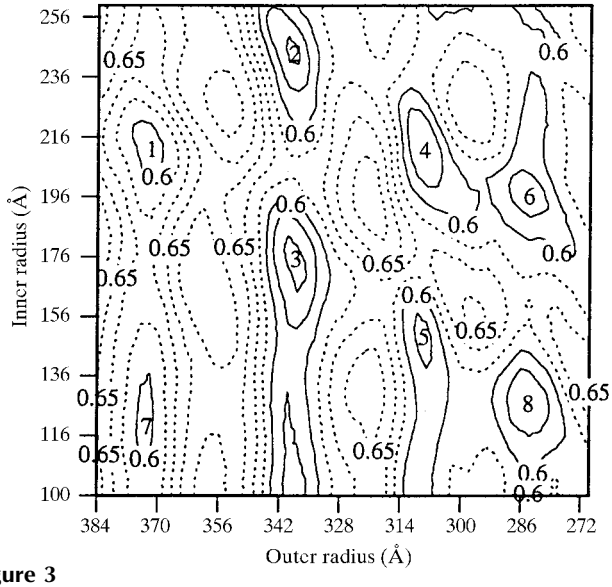

Figure 3
The two-dimensional *R*-factor search using the RDV crystal diffraction data in the resolution range 100–50 Å is given as a function of the inner and outer radii of the spherical-shell model for $\rho'_{NA} = 1.4$. Contours are drawn at an equal interval of 0.0166. Contours lower than 0.6 are drawn in solid lines and those higher than 0.6 in broken lines. The eight local minima are marked by the numbers 1–8. The *R* factor, the inner radius and the outer radius of each minimum are as follows: 1 (0.590, 208 Å, 372 Å), 2 (0.562, 246 Å, 340 Å), 3 (0.562, 172 Å, 338 Å), 4 (0.567, 212 Å, 308 Å), 5 (0.577, 148 Å, 308 Å), 6 (0.573, 198 Å, 284 Å), 7 (0.595, 122 Å, 374 Å) and 8 (0.571, 130 Å, 286 Å).

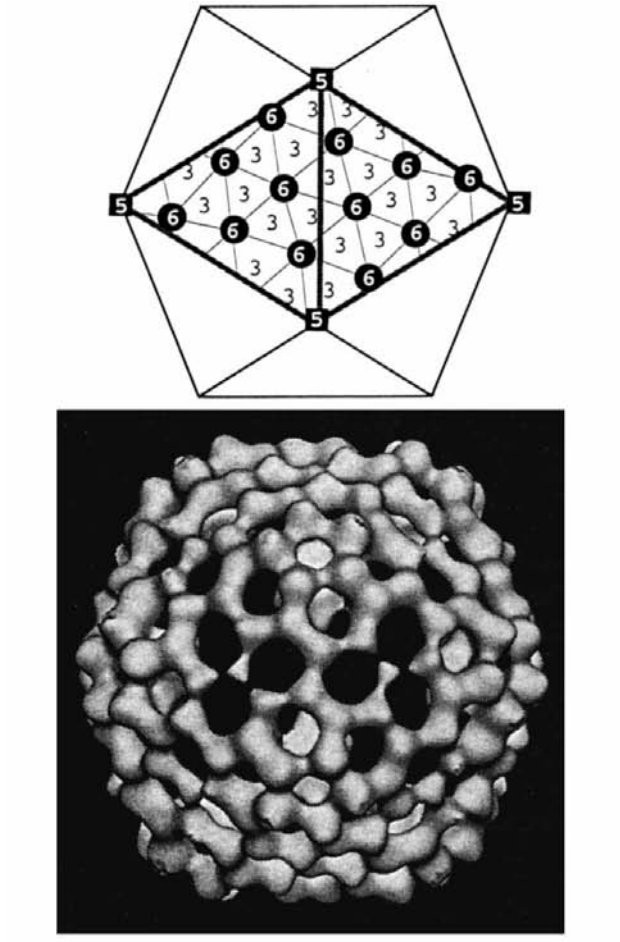

Figure 4
The electron-density map of RDV at the body-centred position calculated with the phases refined by NCSA. (*a*) RDV model with a threshold level of 1σ at 50 Å resolution and the locations of the icosahedral fivefold axes and the quasi-sixfold axes of the $T = 13l$ icosahedral quasi-symmetry are drawn in the lower and the upper parts, respectively. RDV with sections y = 0/128 to 63/128 is shown in this figure. (*b*) The contours of 20 Å are drawn at the 0.8σ level. The cross section of RDV with sections y = 56/128 to 70/128 are superimposed.

the $T = 9$ quasi-symmetry shown in Fig. 5 (Kimura & Shikata, 1968; Uyeda & Shikata, 1982). However, recent electron microscopy of RDV has suggested that it exhibits $T = 13$ quasi-symmetry (Guangying *et al.*, 1995). Outer capsid structures with $T = 13$ quasi-symmetry have been observed by electron microscopy of the genera *Rotavirus* and *Orbivirus* (Hernandez & Akahori, 1986; Ludert *et al.*, 1986; Prasad *et al.*, 1988, 1992). Furthermore, the X-ray structure of *Orbivirus* blue-tongue virus, determined by the group of D. Stuart, Oxford University, exhibits the $T = 13$ quasi-symmetry (Cornuejols, 1996).

The phase extension was initiated using 50 Å resolution phases. After the phase refinement, the NCSA was iterated ten times at the same resolution and the resolution was extended to higher resolution by one reciprocal-cell dimension. The grid sizes of the electron-density maps were 8.5 Å in the resolution ranges 50–25.2 and 6.4–20 Å. The R factor and correlation coefficient at each iteration are plotted in Fig. 6(*a*). Both criteria for the final iteration are also plotted as a function of resolution (Fig. 6*b*). The R factor and correlation coefficient converged to 0.176 and 0.914, respectively, at 20 Å resolution. The electron-density map at 20 Å resolution, shown in Fig. 4(*b*), shows a lump of electron density around each icosahedral fivefold axis inside the capsid outer shell. Another shelled structure with 20 Å thickness appears at the radius of 240 Å.

4. Results and discussion

4.1. Breaking the centre of symmetry using the spherical-shell model

Figs. 7(*a*) and 7(*b*) are the initial and refined phase distributions of the $T = 9$ and $T = 13d$ model crystals. The closed and open blocks represent the initial and refined phases by NCSA phase refinement, respectively. The initial phase angles are all either 0 or 180°. After 200 cycles of phase refinement, the phase distributions are no longer centric. The $T = 9$ model virus is more centric than the $T = 13d$ model virus in phase distribution, because the subunits are centrosymmetrically arranged on the surface of the $T = 9$ model virus. However, in the case of the $T = 13d$ model, the distribution on the surface

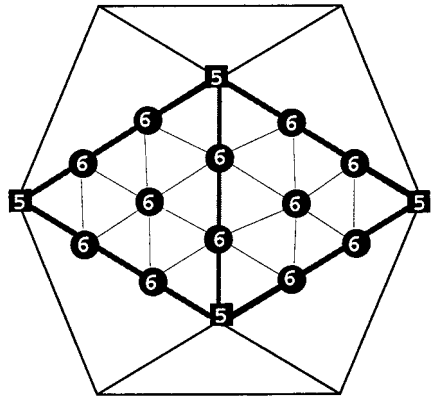

Figure 5
The locations of the icosahedral fivefold and quasi-sixfold axes of the $T = 9$ icosahedral quasi-symmetry.

of the virus is not centrosymmetric, and this difference between the $T = 9$ and $T = 13d$ arrangements may enable us to distinguish clearly the $T = 9$ symmetry from $T = 13$ (d or l) by *ab initio* phasing.

The centric nature of the initial RDV phases from the spherical-shell model has been successfully broken by the NCSA phase refinement. Phase refinement at 50 Å resolution was inspected by comparing phases at each cycle with those of the final cycle at 20 Å resolution and with their enantiomorphs for 909 non-centric reflections. The averaged phase differences of each cycle at 50 Å resolution *versus* those of the final cycle and *versus* their enantiomorphs are shown in Fig. 8. During the first cycles of the refinement, the phase angles are intermediate between those of the final structure and its enantiomorph. This suggests that the first few cycles of the refinement are unable to break the centric nature of the initial phases. After the first few cycles of the phase refinement, the phases begin to approach those of one of the enantiomorphs. Small artificial fluctuations presumably accumulate during the averaging due to computational noise introduced, for example, by the interpolations associated with the averaging. Once the fluctuations have fixed an enantiomorph, the struc-

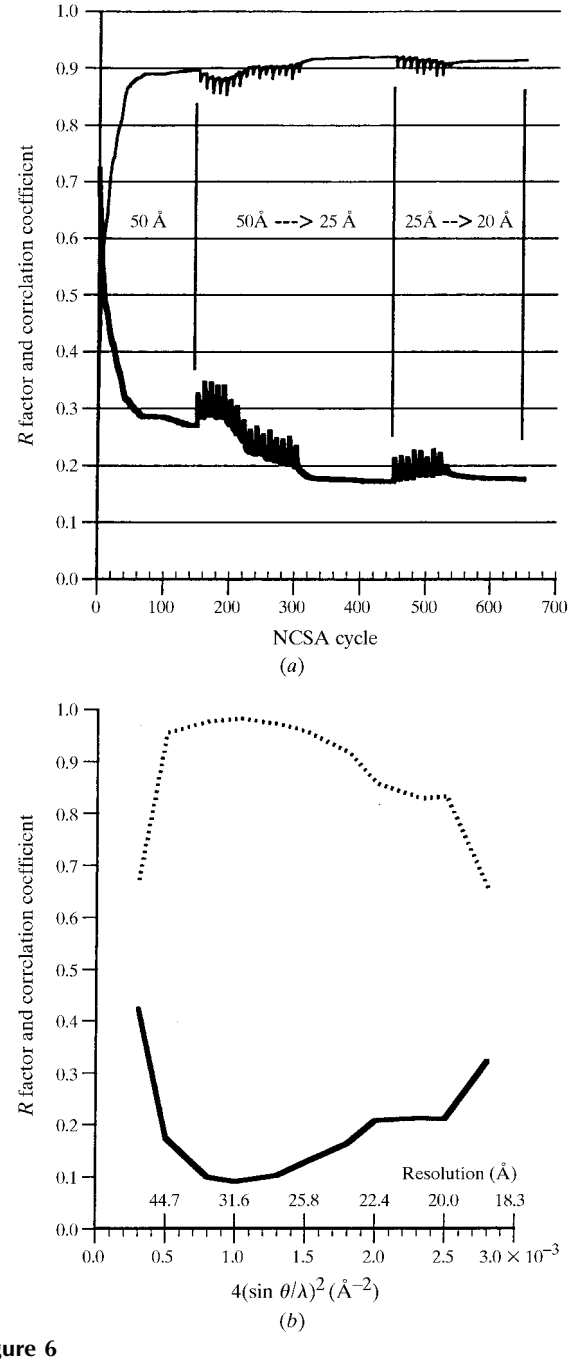

Figure 6
(*a*) The trails of RDV crystal structure analysis by the NCSA. The *R* factor (heavy line) of 0.723 and the correlation coefficient (thin line) of 0.146 at 50 Å resolution at the initial stage were both improved to 0.176 and 0.914, respectively, at 20 Å resolution after 650 iterations. (*b*) *R* factors (heavy line) and correlation coefficients (dotted line) for the final iteration at 20 Å resolution are plotted against $4(\sin\theta/\lambda)^2$ and the resolution.

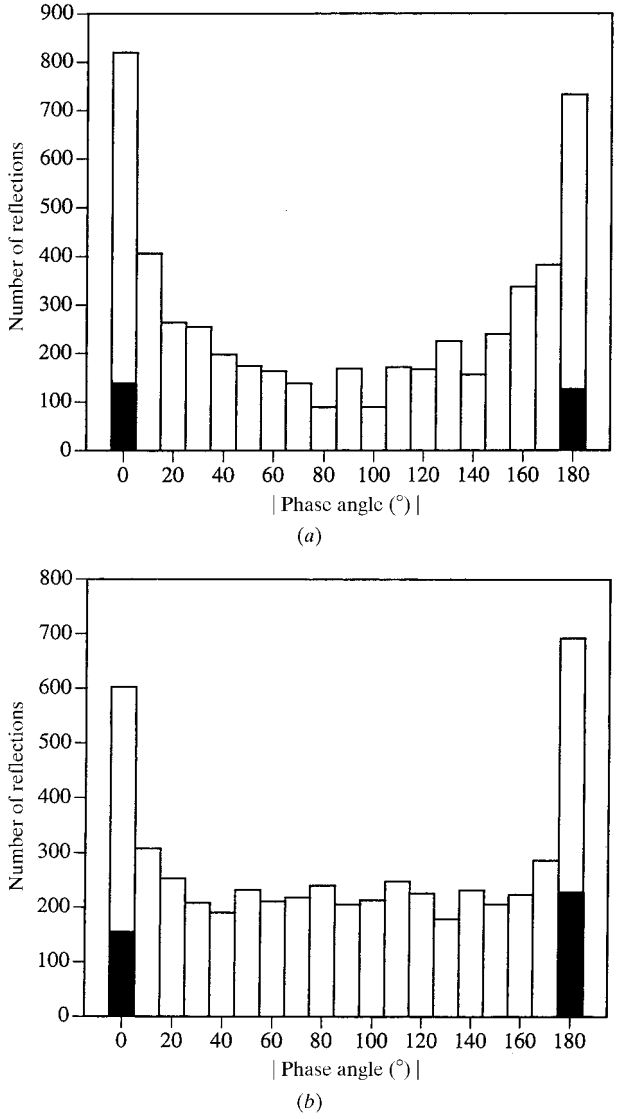

Figure 7
(*a*) The distribution of the phase angles for the $T = 9$ model virus. The closed and open blocks represent initial phases at 85 Å and refined phases at 30 Å resolution, respectively. (*b*) The distribution of the phase angles for the $T = 13d$ model virus. The closed and open blocks represent the initial phases at 76 Å resolution and the refined phases at 30 Å resolution, respectively.

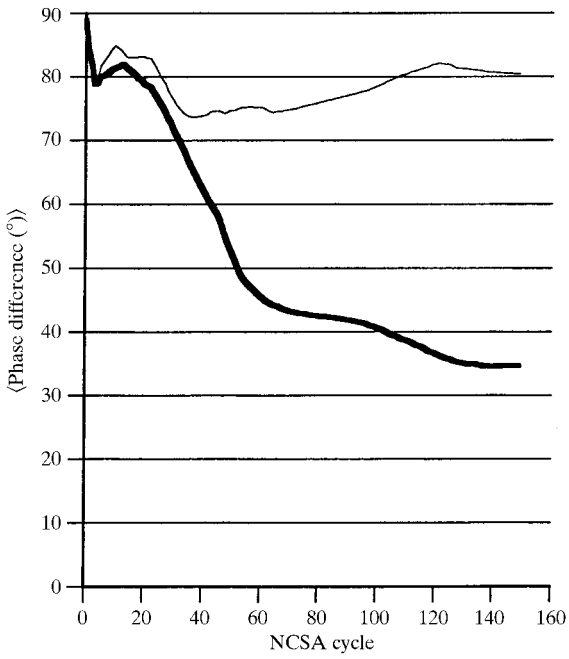

Figure 8
The average phase difference for 909 observed non-centric reflections at 50 Å resolution relative to those of the corresponding reflections of the final structure at 20 Å resolution. The heavy and thin lines represent the refined structure of RDV and its enantiomer, respectively.

tural analysis converges on this enantiomorph. In order to assess the effect of the artificial fluctuations, the NCSA refinement was carried out by introducing asymmetry into the initial phase set. Any similar test calculation achieved faster convergence compared with the ordinary NCSA refinement. These test calculations indicate that the icosahedral NCSA refines the phases correctly by detecting a small shift toward one of two enantiomorphs due to computational noise.

4.2. Structure of RDV

The structural features of RDV are schematically summarized in Fig. 9. The capsid outer shell has $T = 13$ (*d* or *l*) icosahedral quasi-symmetry. There are 20 threefold axes and 240 quasi-threefold axes on the capsid outer shell of the $T = 13$ icosahedral virus. Since the main component of the capsid outer shell is P8 (Omura *et al.*, 1989), capsomers with high electron densities at the quasi-threefold axes are composed of trimers of P8. Electron densities at the threefold axes of the capsid outer shell disappear as the refinement proceeds. P2, essential for RDV infection (Yan *et al.*, 1996), has been eliminated during the RDV purification for the present study. Therefore, P2 might be located at the threefold axes on the capsid outer shell of intact RDV. The core inner shell composed of P3 is distinguished from the capsid outer shell in the electron-density map at 20 Å resolution (Fig. 4*b*). In the RNA region within a radius of 250 Å, ordered structures are visible (Fig. 4*b*). They strongly suggest double-stranded RNA character and define another shell of the RDV. Consequently, the RDV has a triple-shelled structure. Another structural feature is the 12 lumps of electron density inside the core inner

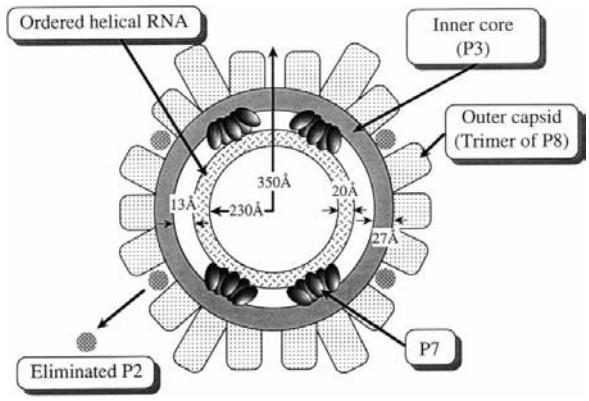

Figure 9
A schematic structural model of RDV obtained by the present structure analysis. The outer radius of about 350 Å, 27 Å thickness of the inner core shell and RNA shell with 230 Å radius and 20 Å thickness were determined from the electron-density map at 20 Å resolution. The capsid outer shell of the intact RDV is composed of P8 trimers at quasi-threefold axes and P2 at threefold axes on the spherical surface of $T = 13$ icosahedron. Broken circles are P2 in the intact RDV. They have been removed from RDV used for the present study. P7 molecules cluster around each fivefold axis inside the core shell.

shell. It seems that each lump has five structural units around an icosahedral fivefold axis. Therefore, it implies that 60 structural units are included in RDV. Analytical electrophoresis has suggested that RDV contains about 60 P7 molecules inside the core inner shell and the molecules can bind RNA (Omura, 1996). Thus, the lumps may be P7 molecules.

Part of this work was performed with the approval of the Photon Factory Advisory Committee (Proposal No. 89-039). TT was supported in part by the 'Research for the Future' Program (No. 96L00503) from the Japan Society for the Promotion of Science, Grant-in-Aids for Science Research on Priority Area (No. 05244103 and No. 06276102) from the Ministry of Education, Science and Culture of Japan, and the TARA project of Tsukuba University.

References

Abad-Zapatero, C., Abdel-Meguid, S. S., Johnson, J. E., Leslie, G. W., Rayment, I., Rossmann, M. G., Suck, D. & Tsukihara, T. (1981). *Acta Cryst.* B**37**, 2002–2018.
Acharya, R., Fry, E., Stuart, D., Fox, G., Rowlands, D. & Brown, F. (1989). *Nature (London)*, **337**, 709–716.
Bernstein, F. C., Koetzle, T. F., Williams, G. J. B., Meyer, E. F. J., Brice, M. D., Rodgers, J. R., Kennard, O., Shimanouchi, T. & Tasumi, M. (1977). *J. Mol. Biol.* **112**, 535–542.
Caspar, D. L. D. & Klug, A. (1962). *Cold Spring Harbor Symp. Quant. Biol.* **27**, 1–24.
Chapman, M. S., Tsao, J. & Rossmann, M. G. (1992). *Acta Cryst.* A**48**, 301–312.
Cornuejols, D. (1996). Editor. *ESRF Highlights* 1995/1996, pp. 53–54. Grenoble: European Synchrotron Radiation Facility.
Green, D. W., Ingram, V. M. & Perutz, M. F. (1954). *Proc. R. Soc. London Ser. A*, **255**, 287–307.

Guangying, L., Zhou, Z. H., Jakana, J., Deyou, C., Shengxiang, C., Xincheng, W., Xiaocheng, G. & Chiu, W. (1995). *High Technol. Lett.* **1**, 1–4.
Harrison, S. C., Olson, A. J., Schutt, C. E., Winkler, F. K. & Bricogne, G. (1978). *Nature (London)*, **276**, 368–373.
Hernandez, F. & Akahori, H. (1986). *Rev. Biol. Trop.* **34**, 89–97.
Inoue, H. & Timmins, P. A. (1985). *Virology*, **147**, 214–216.
Johnson, J. E., Akimoto, T., Suck, D., Rayment, I. & Rossmann, M. G. (1976). *Virology*, **75**, 394–400.
Jurnak, F., Rich, A., van Loon-Klaassen, L., Bloemendal, H., Taylor, A. & Carpenter, F. H. (1977). *J. Mol. Biol.* **112**, 149–153.
Kano, H., Koizumi, M., Noda, H., Mizuno, H., Tsukihara, T., Ishikawa, K., Hibino, H. & Omura, T. (1990). *Nucleic Acids Res.* **18**, 6700.
Kimura, I. & Shikata, E. (1968). *Proc. Jpn Acad.* **44**, 538–543.
Ludert, J. E., Gil, F., Liprandi, F. & Esparza, J. (1986). *J. Gen. Virol.* **67**, 1721–1725.
Luo, M., Vriend, G., Kamer, G., Minor, I., Arnold, E., Rossmann, M. G., Boege, U., Scraba, D. G., Duke, G. M. & Palmenberg, A. C. (1987). *Science*, **235**, 182–191.
Miyahara, J., Takahashi, K., Amemiya, Y., Komiya, N. & Satow, Y. (1986). *Nucl. Instrum. Methods Phys. Res.* **246**, 572–575.
Mizuno, H., Kano, H., Omura, T., Koizumi, M., Kondoh, M. & Tsukihara, T. (1991). *J. Mol. Biol.* **219**, 665–669.
Muckelbauer, J. K., Kremer, M., Minor, I., Diana, G., Dutko, F. J., Groarke, J., Pevear, D. C. & Rossmann, M. G. (1995). *Structure*, **3**, 653–667.
Omura, T. (1996). Personal communication.
Omura, T. & Inoue, H. (1985). CMI/AAB Description of Plant Viruses, No. 296.
Omura, T., Ishikawa, K., Hirano, H., Ugaki, M., Minobe, Y., Tsuchizaki, T. & Kato, H. (1989). *J. Gen. Virol.* **70**, 2759–2764.
Omura, T., Morinaka, T., Inoue, H. & Saito, Y. (1982). *Phytopathology*, **72**, 1246–1249.
Otwinowski, Z. (1993). *Proceeding of the CCP4 Study Weekend: Data Collection and Processing*, edited by L. Sawyer, N. Isaacs & S. Bailey, pp. 56–62. Warrington: Daresbury Laboratory.
Prasad, B. V., Wang, G. J., Clerx, J. P. & Chiu, W. (1988). *J. Mol. Biol.* **199**, 269–275.
Prasad, B. V., Yamaguchi, S. & Roy, P. (1992). *J. Virol.* **66**, 2135–2142.
Rayment, I., Baker, T. S. & Caspar, D. L. D. (1983). *Acta Cryst.* B**39**, 505–516.
Rayment, I., Baker, T. S., Caspar, D. L. D. & Murakami, W. T. (1982). *Nature (London)*, **295**, 110–115.
Rossmann, M. G. (1972). Editor. *The Molecular Replacement Method*. New York: Gordon & Breach.
Rossmann, M. G. (1990). *Acta Cryst.* A**46**, 73–82.
Rossmann, M. G. & Blow, D. M. (1962). *Acta Cryst.* **15**, 24–31.
Sakabe, N. (1983). *J. Appl. Cryst.* **16**, 542–547.
Suzuki, N., Kusano, T., Matsuura, Y. & Omura, T. (1996). *Virology*, **219**, 471–474.
Suzuki, N., Tanimura, M., Watanabe, Y., Kusano, T., Kitagawa, Y., Suda, N., Kudo, H., Uyeda, I. & Shikata, E. (1992). *Virology*, **190**, 240–247.
Tsao, J., Chapman, M. S. & Rossmann, M. G. (1992). *Acta Cryst.* A**48**, 293–301.
Tsao, J., Chapman, M. S., Wu, H., Agbandje, M., Keller, W. & Rossmann, M. G. (1992). *Acta Cryst.* B**48**, 75–88.
Uyeda, I. & Shikata, E. (1982). *Ann. Phytopathol. Soc. Jpn*, **48**, 295–300.
Valegård, K., Liljas, L., Fridborg, K. & Unge, T. (1990). *Nature (London)*, **345**, 36–41.
Yan, J., Tomaru, M., Takahashi, A., Kimura, I., Hibino, H. & Omura, T. (1996). *Virology*, **224**, 539–541.